Sustainable Transportation Solutions in Remote Areas: Static Analysis of Vertical Axis Wind Turbines for Enhanced Efficiency of Wind-Powered Cars

Youssef Kassem
Department of Mechanical Engineering, Engineering Faculty, Near East University, Nicosia, Cyprus | Energy, Environment, and Water Research Center, Near East University, Nicosia, Cyprus | Research Center for Science, Technology and Engineering (BILTEM), Near East University, Nicosia, Cyprus
yousseuf.kassem@neu.edu.tr (corresponding author)

Huseyin Camur
Department of Mechanical Engineering, Engineering Faculty, Near East University, Nicosia, Cyprus | Research Center for Science, Technology and Engineering (BILTEM), Near East University, Nicosia, Cyprus
huseyin.camur@neu.edu.tr

Almonsef Alhadi Salem Mosbah
High and Intermediate Institute of Agricultural Technology, Gheran, Libya
almonsef4400@gmail.com

Received: 25 July 2024 | Revised: 24 November 2024 | Accepted: 27 November 2024

 DOI: https://doi.org/10.48084/etasr.8517

ABSTRACT

It is imperative that a sustainable transportation system, powered by renewable energy resources, be implemented in order to mitigate the impacts of climate change and enhance living standards. A Wind-Powered Car (WPC) is a vehicle that employs a connection between the vehicle and wind turbine blades, thereby leveraging the advantages of wind kinetic energy. The energy is then conveyed directly to the car's wheels via a system of mechanical connections and gears, enabling the vehicle to move without the use of fossil fuels. The absence of an internal combustion engine results in the generation of negligible emissions. The primary objective of this study is to examine the static aerodynamic drag of nine WPC designs with diverse blade configurations of Vertical Axis Wind Turbines (VAWT). To achieve this objective, Autodesk Computational Fluid Dynamics (CFD) was employed to model the aerodynamic drag of WPC designs at varying wind speeds of 4 m/s, 6 m/s, and 8 m/s. The comparative analysis revealed that model 8, featuring a 3-blade Savonius wind turbine without a circular end plate, demonstrated superior efficiency among all car models. This is evident in its ability to generate the highest mechanical power compared to other blade designs. These findings contribute to the understanding of aerodynamic performance in VAWT cars, offering valuable insights for further design optimization. Furthermore, the results highlight model 8 as a promising solution for sustainable transportation, aligned with SDG 7 and SDG 11, through the development of clean and efficient wind-powered vehicles.

Keywords-vertical axis wind turbine; wind energy; wind-powered car; aerodynamic simulation; SDG 7; SDG 11

I. INTRODUCTION

The necessity of energy has been a critical aspect of human history, traditionally fulfilled by conventional fossil fuels. Nevertheless, the environmental consequences of fossil fuel utilization, including pollution and climate change due to greenhouse gas emissions, have prompted scientific researchers to pursue alternative, sustainable energy sources [1-4]. The objective is to generate energy in a manner that causes minimal environmental harm. A substantial body of research has underscored the significance of renewable energy sources, such as wind power, in reducing greenhouse gas emissions [5-8]. In recent times, wind power has attracted considerable attention as

a prominent, economically viable, and environmentally friendly renewable energy source. The potential of wind power lies in its ability to harness kinetic energy from wind to generate electricity, offering a sustainable alternative to traditional fossil fuel-based power generation [9, 10]. In general, wind energy is converted to mechanical energy and subsequently to electrical energy through the use of a wind turbine [11]. Wind energy can be utilized as a power source for WPC [12]. In the field of vehicle design, aerodynamics represents a particularly crucial area of consideration [13]. The field of aerodynamics is concerned with the study of the movement of air around a solid object, such as a car [13]. The configuration of the vehicle is a pivotal factor that affects its aerodynamic properties [14, 15]. In particular, the aerodynamic forces, including drag, are of great consequence in estimating the performance of a vehicle on the road, particularly in regard to overcoming air resistance [14, 15]. Minimizing drag through the implementation of an efficient aerodynamic design is a fundamental aspect of enhancing the overall performance and efficiency of WPC [16]. This convergence of renewable energy and aerodynamic principles highlights the interdisciplinary nature of developing innovative and sustainable transportation solutions.

A. Related Works

A number of studies have been conducted, both theoretically and numerically, with the objective of designing a wind-powered car. Authors in [17] estimated and compared the characteristics of drag force and torque of three C-section-blade and NACA0012-blade wind cars using a velocity analysis approach. In a further study, authors in [18] determined the torque and aerodynamic forces (lift and drag forces) for vertical axis wind turbine cars with various blade models (NACA 0012 and NACA 2412). Authors in [19] developed a wind turbine with the specific purpose of serving as a power source, generating electrical charge for car batteries while the vehicle is in motion. Furthermore, authors in [20] conducted an estimation of the mechanical power produced by a single large C-section of a vertical wind turbine designed for wind-powered cars. The study involved a comparison of the results obtained from a configuration comprising three C-section blades and another configuration comprising three double C-section blades. In a further study, authors in [21] investigated the aerodynamic effects on the performance of Savonius turbine-powered cars using the velocity analysis method. The findings indicated that the greatest mechanical power output for the WPC was achieved when the Savonius wind turbine with a gap was employed. Authors in [22] employed Autodesk CFD to examine the aerodynamic characteristics of three models of a vertical axis wind turbine car, namely NACA 0012 with an angle of contact of 2°, a large single C-section, and C-section blades. The objective was to quantify the drag force for each model. Authors in [23] designed a Savonius vertical axis wind turbine with the specific intention of charging up to four cell phone batteries, with a total electrical output of 60W, for use in vehicles. Authors in [24] investigated the impact of blade number and size, particularly the use of NACA 0012 blades, on the mechanical power of wind turbine-powered cars. The analysis, conducted through velocity analysis methods, demonstrated that an increase in the size and number of NACA 0012 blades resulted in enhanced mechanical power production in wind turbine-powered cars. This enhancement was observed while maintaining effectiveness at the same wind speed and angle of attack. Moreover, a number of prototypes have been developed with the objective of examining the concept of WPC. The Greenbird, a purpose-built vehicle designed by Richard Jenkins, set land speed records in 2009, reaching an average speed of 126.2 mph (202.9 km/h) across Nevada's Ivanpah Dry Lake [25]. In a notable achievement, a team of Dutch students developed the Ventomobile, a vehicle featuring a lightweight design and a front-mounted turbine. This innovative approach showcased the vehicle's ability to use both solar and wind energy for propulsion in the World Solar Challenge's Cruiser Class [26]. In 2010, the Wind Explorer team developed the Blackbird WPC, a lightweight, aerodynamic vehicle that completed a 3,000-kilometer journey across Australia, primarily relying on wind power with minimal battery assistance. The Nemesis, an electric vehicle powered by wind, was designed by the UK-based company Ecotricity and achieved a UK land speed record in 2010 with a top speed of 151 mph (244 km/h) [28]. These developments indicate the potential of wind energy as a sustainable and high-speed transportation source.

B. Scope of the Study

The present study seeks to examine the static aerodynamic forces, mechanical torque, and power associated with a range of wind-powered vehicle configurations, with a view to aligning the findings with the overarching objectives of sustainable development. Nine VAWT models, each with a distinct proposed design, were subjected to static simulation using Autodesk CFD. A numerical estimation of aerodynamic drag, encompassing both the drag force and the coefficient, was conducted at varying wind speeds 4 m/s, 6 m/s, and 8 m/s. Building upon prior studies, this investigation focuses on the refinement of features with the objective of enhancing vehicle performance and efficiency, thereby contributing valuable insights to the advancement of sustainable wind-powered transportation solutions.

II. MATERIALS AND METHODS

In order to obtain the aerodynamic parameters, which include the drag coefficient and drag force, a numerical model was employed. The model guarantees independence from time-step size, convergence limits, and other pertinent modeling conditions. The study employs a three-dimensional CFD simulation model constructed using AutoCAD software, as presented in Figure 1.

A. Wind-Power Car (WPC)

Wind energy represents the primary source of energy for the WPC. The vehicle is attached to the wind turbine blades, thereby capitalizing on the advantages of the wind's kinetic energy. The blades are directly connected to the wheels through various couplings, employing bevel gears to convert the wind's kinetic energy into mechanical energy and overcome the low-speed resistance on the main shaft. The gears are of great importance in the conversion of wind energy into mechanical energy, thus facilitating the overcoming of the loads exerted on the main shaft. In this study, nine WPC designs with distinct

blade shapes of vertical axis wind turbines were proposed, as illustrated in Table I. Furthermore, Figure 2 shows the wind car connected to Savonius wind turbines with two and three blades, showcasing distinct arc bucket angles, as seen in Figure 3. Additionally, Figure 4 presents the models of the vertical wind rotor, which was designed for vertical axis wind turbines. The models exhibit a variety of blade types, including NACA airfoils with a 2° angle of attack, C-section blades, and large single C-section blades. It is noteworthy that the NACA airfoil and C-section blades are oriented at an angle of 120°.

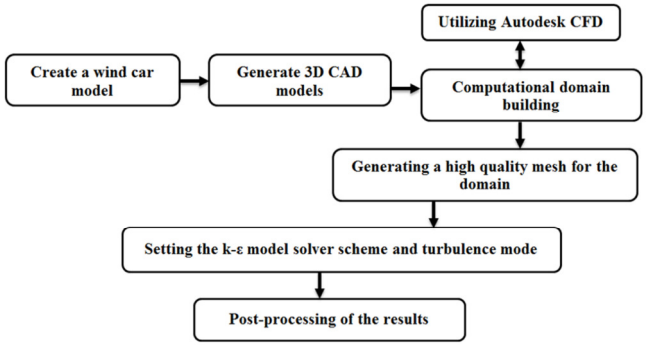

Fig. 1. The procedure of the proposed methodology.

TABLE I. CAR MODELS AND DESCRIPTION

Model	Description of wind turbine model used
Model 1	2-blade Savonius wind turbine with circular end plate and arc bucket angle 60°
Model 2	2-blade Savonius wind turbine with circular end plate and arc bucket angle 90°
Model 3	2-blade Savonius wind turbine with circular end plate and arc bucket angle 120°
Model 4	3-blade Savonius wind turbine with circular end plate and arc bucket angle 60°
Model 5	3-blade Savonius wind turbine with circular end plate and arc bucket angle 90°
Model 6	3-blade Savonius wind turbine with circular end plate and arc bucket angle 120°
Model 7	NACA airfoils with a 2° angle of attack
Model 8	3-blade Savonius wind turbine without circular end plate
Model 9	3-blades large single C-section blades without circular end plate

The dimensions of the vehicle body are 2.2 m in height, 1.8 m in width, and 4.5 m in length. The NASA airfoil rotor is defined by a chord length of 0.3 m and a height of 2 m. Moreover, the rotor radius of one meter indicates that the rotor blades extend outward to a maximum distance of one meter from the central axis. The rotor's thickness of 0.015 m has been designed with the objective of achieving an optimal balance between aerodynamic performance and structural strength. Moreover, the dimensions of a C-section, are designed with a thickness of 0.015 m, a rotor radius of 1 m, and a height of 2 m.

B. Simulation Model

This study employs Autodesk CFD software for numerical simulations, applying the Navier-Stokes equations and the realizable *k-ε* turbulence model to analyze the aerodynamic drag and streamline flow characteristics of a vertical axis wind turbine car. The study's primary focus is on pressure, velocity distributions, and aerodynamic drag, employing characteristic-based velocity inflow/outflow and external flow/static simulation settings. In the study of automobile drain fields, the fluid is typically assumed to be incompressible, isothermal, and adiabatic. This is done in accordance with the principles of turbulent flow as set forth by the Navier-Stokes (NS) equations, which are accepted viscous fluid dynamics equations.

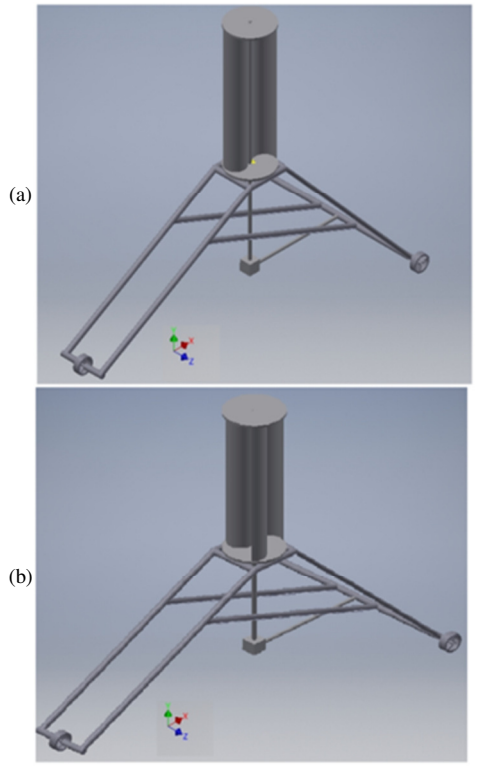

Fig. 2. Wind car model connected to; (a) 2-blade Savonius wind turbine and (b) 3- blades Savonius wind turbine.

The fluid is modeled as a three-dimensional unsteady flow of an ideal gas. The governing equations for control in this context involve the NS equations, reflecting the continuum assumption and addressing the complexities of turbulent flow in the automobile drain field as:

$$\frac{\partial \rho}{\partial t} + \frac{\partial (\rho u_i)}{\partial x_j} = 0 \quad (1)$$

$$\frac{\partial}{\partial t}(\rho \bar{u}_i) + \bar{u}_j \frac{\partial}{\partial x_j}(\rho \bar{u}_i) = -\frac{\partial \bar{p}}{\partial x_i} + \mu \frac{\partial^2 \bar{u}_j}{\partial x_i \partial x_j} - \frac{\partial \overline{u_i u_j}}{\partial x_j} + \bar{f}_i \quad (2)$$

$$P = \rho R T \quad (3)$$

where x_i, x_j, and t are Euler variables, ρ is air density, u is the velocity of the fluid, μ is the coefficient of dynamic viscosity, P is the pressure in the flow field, R is the universal gas constant and T is the temperature in the flow field. The incorporation of a Reynolds stress term into the modified NS equation introduces a degree of complexity, thereby rendering it non-closed. To address this issue, a variety of turbulence models are employed for closure purposes. Common methods include the standard *k-ε* model, the Shear-Stress Transport

(SST) turbulence model, and the Renormalization Group (RNG) turbulence model. These turbulence models provide closure by incorporating additional equations to account for the Reynolds stresses, thereby enabling a more comprehensive and solvable representation of turbulent flow in the context of the automobile drain field [22].

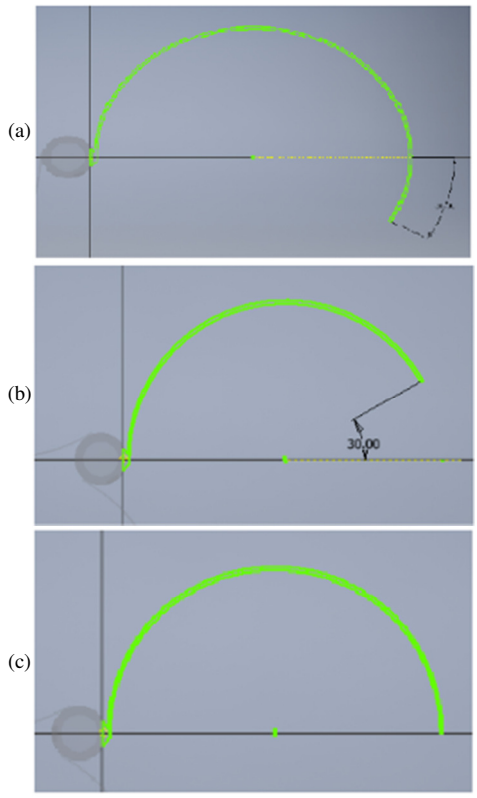

Fig. 3. Schematic diagram of Savonius blades with various arc bucket angles; (a) 120°, (a) 60° and (a) 90°.

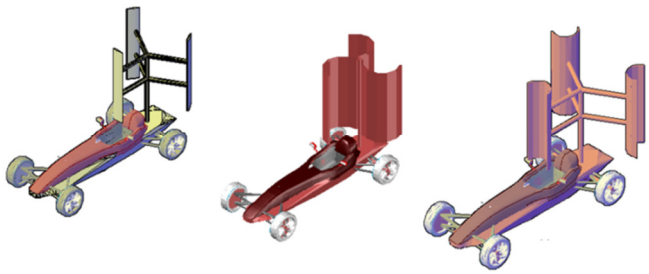

Fig. 4. Wind car model connected to NACA airfoils with a 2° angle of contact (left), C-section blades (middle), and large single C-section blades (right).

The standard *k-ε* turbulence model is semi-empirical, solving approximate conservation equations for turbulent kinetic energy (*k*) and its dissipation rate (*ε*). The transport equations for *k* and *ε* can be derived from the NS equation, but they include unknown terms representing correlations of fluctuating terms. Empirical modeling, based on physical reasoning, is used for some terms, while others are neglected, introducing empiricism and potential accuracy limitations in turbulence models. The transport equation for *k* closely resembles its exact form, but the same cannot be said for the *ε*-equation [22]. The term that represents the production of turbulence is:

$$\rho\frac{\partial}{\partial t}(k)+\rho\bar{u}_i\frac{\partial}{\partial x_j}(k)=\frac{\partial}{\partial x_j}\left[\left(\frac{\mu+\mu_t}{\sigma_k}\right)\frac{\partial k}{\partial x_j}\right]+P-\rho\varepsilon \quad (4)$$

$$P=(\mu+u_t)\left(\frac{\partial u_i}{\partial x_j}+\frac{\partial u_j}{\partial x_i}\right)\frac{\partial u_i}{\partial x_j} \quad (5)$$

and the diffusion equation, ε is

$$\rho\frac{\partial}{\partial t}(\varepsilon)+\rho\bar{u}_i\frac{\partial}{\partial x_j}(\varepsilon)=\frac{\partial}{\partial x_j}\left[\left(\frac{\mu+\mu_t}{\sigma_\varepsilon}\right)\frac{\partial \varepsilon}{\partial x_j}\right]+C_{\mu 1}\frac{\varepsilon}{k}(P)-C_{\mu 2}\frac{\varepsilon}{k}\rho\varepsilon \quad (6)$$

where $C_{\mu 1}=1.44$ and $C_{\mu 2}=11.92$ are constants. ($\sigma_k=1.0$ and $\sigma_\varepsilon=1.3$ are the turbulent Prandtl numbers for *k* and *ε* respectively. Furthermore, turbulent viscosity is computed using [22]:

$$\mu_t=\rho C_\mu\frac{k^2}{\varepsilon}\ ;\ C_\mu=0.09 \quad (7)$$

In developing the standard *k-ε* model, certain terms are determined through simple experiments, while others are optimized to yield optimal results for various benchmark cases. The model is predicated on the assumption that the flow is fully turbulent and that the effects of viscosity can be disregarded. Consequently, the standard *k-ε* model is applicable to fully turbulent flow scenarios. Furthermore, the computational domain in this study is a simplified representation of the physical domain, with specified boundary conditions that dictate fluid entry or exit points set as pressure, mass flow, volume flow, or velocity. Inlet velocities of 4 m/s, 6 m/s, and 8 m/s were applied, thereby influencing the fluid dynamics within the system.

C. Boundary Conditions and Meshes

It is of significant importance to accurately model the external aerodynamic flow in a WPC installed with VAWT blades that are subject to precise boundary conditions and meshing in CFD simulations. The velocity inlet, also referred to as an inlet boundary condition, plays a critical role in defining the manner in which air flows within the simulation area. To demonstrate the impact of varying flow conditions on the object of interest, a series of wind speed scenarios were employed, with speeds of 4 m/s, 6 m/s, and 8 m/s. This method can be used to ascertain the aerodynamic performance under disparate wind conditions, thereby reflecting environmental alterations with precision. Furthermore, to accurately represent real-world scenarios, the airflow entering the inlet must be aligned with the direction of the wind approaching the WPC. This alignment is of significant importance, as it has a direct impact on the separation of flow, vortex formation, and pressure distribution around the vehicle. An accurately specified inlet condition leads to an accurate estimation of aerodynamic forces and thus enhances the credibility of the evaluation of the performance of the WPC. In addition, a pressure outlet is defined in the simulation with a constant gauge pressure of 0 Pa, thereby imitating an open, distant atmosphere in which air can move out of the modeling space. The use of such boundary conditions in external flow simulations is often motivated by the need to prevent the return

flow from the domain from being misdirected, as this can lead to distortions in the results and a reduction in the precision of the aerodynamic predictions. The fixed pressure outlet guarantees the maintenance of a genuine pressure field within the domain, thus facilitating the simulation of wake effects and the pressure recovery zone situated behind the vehicle.

Furthermore, no-slip wall conditions are imposed on the entire surface area of WPC and VAWT blades. A zero relative air velocity at the surface of a car is indicative of the perfect imitation of the no-slip phenomenon, whereby air particles in close proximity to solid surfaces adhere to them. This is significant in comprehending the impact of surface roughness and shape on aerodynamic drag and lift, as well as in simulating boundary layer formation. It is therefore crucial to provide an accurate description of the wall boundaries in order to predict the aerodynamic forces and moments that directly affect the stability and efficiency of WPCs. Furthermore, tetrahedral meshes are typically employed in CFD simulations when the flow is external, given their capacity to accommodate complex geometries, as is the case for WPC and VAWT blades. This renders them highly useful in exterior aerodynamic studies, as they can be adapted to different surface configurations and are more straightforward to manipulate around intricate shapes. The tetrahedral mesh type is of particular significance in the context of resolving vortices and other intricate flow features that exert a considerable influence on aerodynamic efficiency. This is due to the fact that it permits a comprehensive and detailed capture of the flow in the sharp corners and edges of VAWT blades. To guarantee the veracity of CFD simulation results, including those pertaining to aerodynamic drag (including both the drag force and coefficient), it is essential to conduct a mesh independence study. The objective of this research is to modify the mesh in a manner that will prevent any significant alterations in the outcomes, thereby demonstrating that the solution state is independent of the grid. To validate the CFD model, a mesh independence study must be conducted to ensure that the aerodynamic parameters predicted by the simulation are accurate and reliable, without any reference to mesh artifacts. Furthermore, in order to gain a comprehensive understanding of the aerodynamic performance of these vehicles in an ever-changing wind environment, it is essential to investigate how their surrounding airflow dynamics evolve over time. Therefore, transient simulations are used to examine vortex shedding, flow separation, and reattachment, which are fundamentally unsteady occurrences that significantly influence WPC stability and efficiency.

D. Mechanical Torque Calculation

In general, a VAWT is distinguished by a design wherein the drag force plays a more prominent role than the lift force in the capture of wind energy [29]. Accordingly, the principal objective of the numerical simulations conducted in this study is to ascertain the magnitude of the drag force (F_d) exerted on the blades. With the F_d, it is possible to obtain mathematically the values of the mechanical torque (T_m). The T_m of a rotor can be expressed mathematically as [30, 31]:

$$T_m = F_d \times r \quad (8)$$

$$F_d = \frac{1}{2} \times \rho \times A \times v^2 \times C_d \quad (9)$$

where ρ is the air density (it is assumed to be 1.23 kg/m^3), A is the swept area of the turbine ($A = \pi r^2$), v is the wind velocity, C_d is the drag coefficient of the turbine blades and r is the radius of the turbine blades.

E. Mechanical Power Calculation

The power available at the rotor can be calculated from the mechanical torque and angular velocity (ω) using [32, 33]:

$$P_m = T_m \times \omega \quad (10)$$

The angular velocity of a wind turbine rotor can be estimated using the tip speed ratio and the wind velocity. The tip speed ratio is defined as [30-33]:

$$\lambda = \frac{\omega r}{v} \quad (11)$$

Generally, the average λ for wind turbines can vary depending on the specific design, type of turbine, and its intended application [34]. However, there are general ranges that are commonly observed in practice.

III. RESULTS

A. Characteristics of Streamlines Flow

In general, the visualization of streamlined flows facilitates the tracing of the paths traversed by air particles as they move over the surfaces of vehicles and wind turbines. By observing these streamlines, regions of high and low velocity, pressure variations, and areas where the flow may separate from the surfaces can be identified. Furthermore, an understanding of the streamlines facilitates the optimization of the design, which in turn improves the aerodynamic efficiency, reduces drag, and enhances overall performance [35, 36]. Furthermore, the aerodynamic drag curve, which includes the drag force and drag coefficient, provides quantitative data on the resistance these objects experience due to air resistance [37, 38]. This information is crucial for assessing the energy efficiency of vertical axis wind turbines and cars. The maximum static pressure and speed of the models are presented in Table II.

TABLE II. MAXIMUM VELOCITY AND PRESSURE DISTRIBUTION FOR ALL MODELS UNDER VARYING WIND SPEEDS

Model	**Average maximum wind speed (m/s)**			**Average maximum pressure (Pa)**		
	4 (m/s)	6 (m/s)	8 (m/s)	4 (m/s)	6 (m/s)	8 (m/s)
Model 1	5.05	7.56	10.10	10.09	22.74	40.28
Model 2	5.02	7.55	10.07	10.36	23.23	41.68
Model 3	4.99	7.50	10.01	9.55	21.15	38.10
Model 4	5.10	7.61	10.14	11.23	24.64	43.89
Model 5	4.96	7.46	9.94	11.39	25.57	45.14
Model 6	4.98	7.48	9.97	11.02	24.75	44.03
Model 7	6.58	10.42	14.15	8.81	19.67	35.27
Model 8	5.62	9.20	12.67	9.22	20.95	40.08
Model 9	5.16	7.97	10.41	9.67	21.34	38.20

It was observed that the maximum static pressure was present at the point where the flow stream met the blade surface perpendicularly. The streamlines depicted the trajectories of particles, with coloration indicating both velocity

and pressure. The flow remained attached over the entire profile, separating at the wind turbine's rear end. A turbulent low-pressure wake, characteristic of a notchback wind car, was evident. The highest velocity regions were observed, particularly on the side of the blade experiencing pressure. In contrast, the area of the rotor located at the rear exhibited the lowest velocity, creating a vacuum. In general, the pressure difference across the rotor is a significant factor that affects its performance. This is related to the aerodynamic forces acting on the blades, which in turn affect the torque and power generated by the turbine. A higher-pressure difference is indicative of the turbine capturing a greater quantity of wind energy and subsequently converting it into mechanical power. Accordingly, model 8 displayed a greater turbulent pressure wake than the other models. Figure 5 shows the streamlined flow and aerodynamic drag curves for model 8.

(a)

(b)

(c)

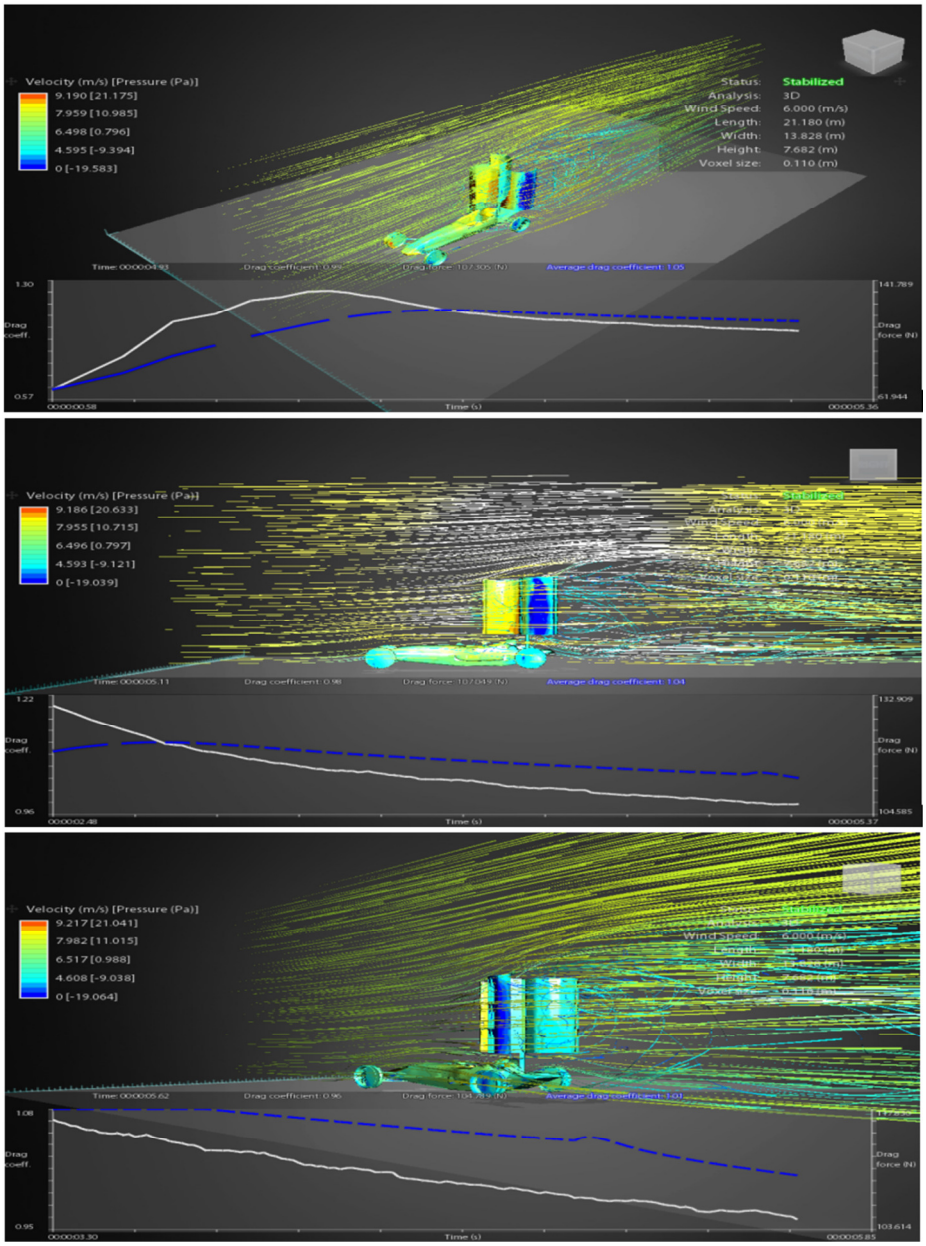

Fig. 5. Streamlines and aerodynamic drag curves for model 1 car at 4 m/s (white curve: drag force; blue curve: drag coefficient), (a) front, (b) profile, (c) back.

B. Drag Force and Coefficients

In this study, numerical estimations were conducted to determine the drag force and coefficients for various models of cars equipped with vertical-axis wind power turbines. Figure 6 presents the estimated values of the drag coefficient (C_d) and drag force (F_d) across all models. The analysis reveals that the drag coefficient values exhibit a range of 0.63 to 1.00. This range indicates the efficiency of the cars in overcoming air resistance, with lower values generally suggesting superior

aerodynamic performance. Moreover, the study reveals that model 7 and model 9 exhibit the highest and lowest drag coefficient values, respectively. Furthermore, the results indicate that in the study, the highest and lowest values of drag force are observed for model 3 (F_d = 14.45 N at 4 m/s) and model 8 (F_d = 170.96 N at 8 m/s), respectively, under different velocities, as shown in Figure 6. The observed variation in drag force can be attributed to the differences in design and aerodynamic characteristics among the various car models.

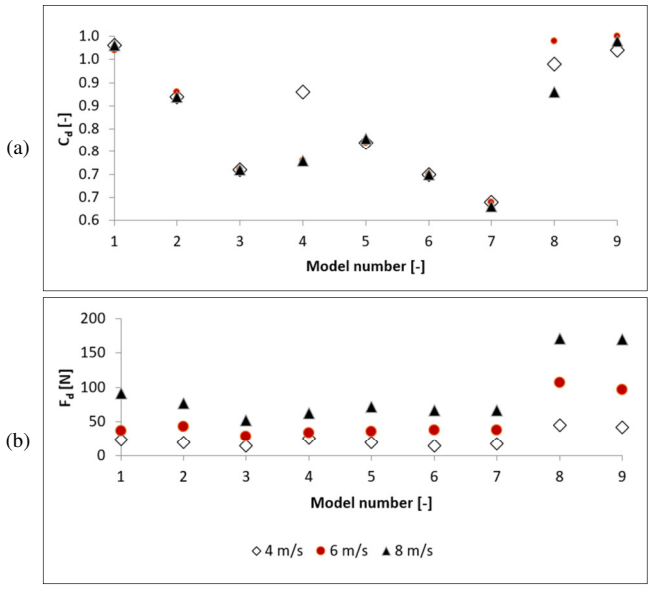

Fig. 6. (a) Drag coefficient, (b) drag force, under different velocities for all car models.

The drag force is influenced by a number of factors, including the shape of the vehicle and the surface roughness [39]. In this context, model 3 appears to have a more aerodynamically favorable design at the given velocities, resulting in a lower drag force of 14.45 N. Conversely, model 8 seems to experience higher air resistance, leading to a higher drag force of 170.96 N. Additionally, it can be observed that as the wind velocity increases, the drag force also increases. This is a typical occurrence in the field of aerodynamics. The drag force acting on a moving object, such as a car with wind turbines in this study, tends to increase with higher velocities [39].

C. Mechanical Torque and Power

In this study, the T_m and P_m of rotors are calculated mathematically using (8) and (10), respectively, under varying wind velocities. In the context of wind turbines, the tip velocity ratio is generally regarded as an important parameter. This represents the ratio of the tangential velocity of the blade tips to the wind speed. Modifying the tip speed ratio enables an investigation of the energy capture efficiency of a wind turbine at varying rotation speeds [40]. Accordingly, the P_m is estimated under varying tip speed ratios. The findings of the study indicate that model 8 has been identified as the model that produces the maximum mechanical torque and power among the models under investigation, as shown in Figures 7 and 8. Furthermore, it is notable that as wind velocity increases, both the mechanical torque and power also increase. The observation that model 8 exhibits the highest mechanical torque and power suggests that its design or configuration is particularly effective in harnessing wind energy and converting it into mechanical power. This could be attributed to various factors, such as the aerodynamic design, the efficiency of the rotor, or other specific features of model 8.

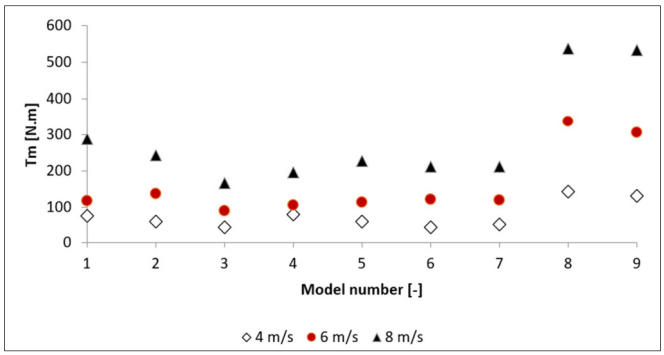

Fig. 7. Mechanical torque under different velocities for all car models.

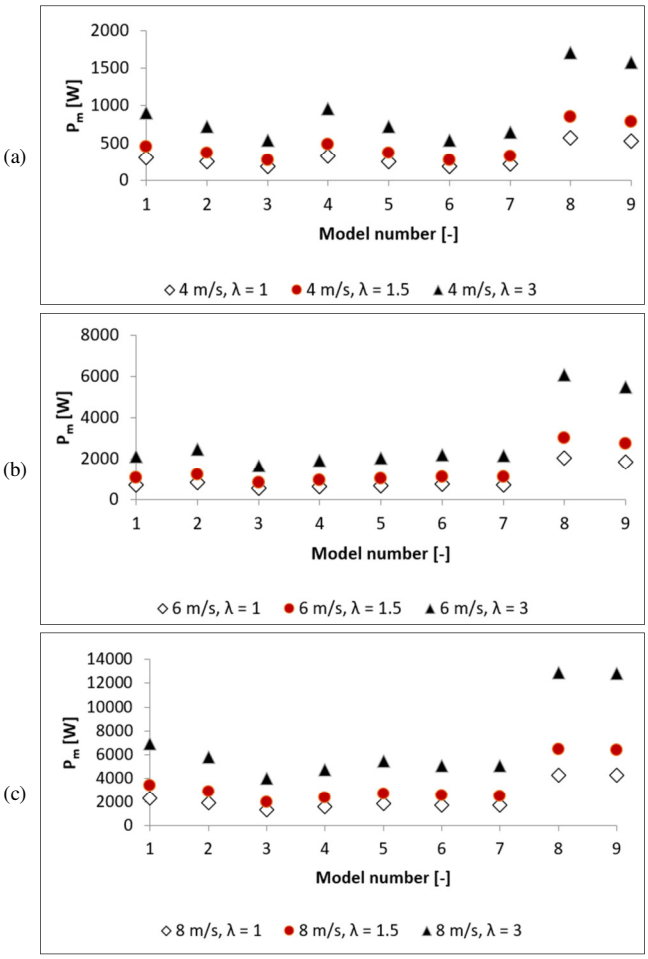

Fig. 8. Mechanical power under different velocities for all car models, (a) 4 m/s, (b) 6 m/s, (c) 8 m/s.

IV. DISCUSSION AND CONCLUSIONS

Wind energy represents a significant renewable resource, offering a means of minimizing the environmental impact of human activities by reducing reliance on non-renewable fossil fuels. In addition to this, wind energy possesses a number of other valuable characteristics. Due to their ability to capture air from all directions, Vertical Axis Wind Turbines (VAWTs) are particularly well-suited for use in remote geographical areas. In this regard, nine VAWT automobile models were subjected to static simulation to investigate the effect of aerodynamic drag at three different wind speeds (4 m/s, 6 m/s, and 8 m/s) using Autodesk Computational Fluid Dynamics (CFD). The results demonstrated that model 8 achieved remarkable aerodynamic efficiency through the implementation of key design features. In accordance with the findings presented by authors in [41, 42], the removal of the circular end plate has been shown to reduce drag and the formation of tip vortices, while simultaneously ensuring a cleaner airflow separation and a reduction in turbulence. Furthermore, the augmented torque stability and aerodynamic equilibrium of the three-blade configuration facilitate uniform wind interaction and diminished energy fluctuations [43, 44]. Furthermore, the optimized blade geometry, which increases wind exposure, results in an additional increase in lift and energy conversion. Furthermore, the use of lightweight materials, such as PVC, allows for enhanced responsiveness to varying wind speeds by reducing inertia [45]. The aforementioned evidence suggests that this design is a reliable wind energy option due to its exceptional efficiency, eliminating the necessity for end plates.

The practical deployment of Wind-Powered Cars (WPC) in remote locations necessitates the resolution of several substantial challenges, including energy efficiency, wind availability, and the establishment of an appropriate infrastructure. In order to maximize the production of power during periods of low wind speed, it is necessary for automobiles to be equipped with high-efficiency VAWTs [46, 47]. Authors in [48] have observed, that enhancing energy conversion without compromising vehicle performance necessitates the integration of aerodynamic designs and lightweight materials. It is imperative that dependable, low-maintenance systems be implemented, as repair facilities may be scarce in remote locations. Additionally, hybrid systems that integrate wind with solar or battery storage are necessary for reliable operation, as wind is inherently unpredictable [49]. The resolution of these concerns ensures the economic and environmental viability of the proposed solution. The concept of vehicles powered by VAWTs offers promising potential for further applications, particularly in terms of converting wind energy for stationary energy requirements in rural areas and various forms of transportation. In conclusion, the knowledge gained from these findings is vital for understanding the aerodynamics of VAWT-powered cars and the potential for optimizing their design. Model 8 is one example of how sustainable transport development can contribute to achieving SDG 7 (access to affordable and clean energy). Furthermore, a wind-powered car using VAWTs offers an inexpensive yet environmentally friendly option for developing countries facing the challenge of providing affordable and sustainable energy.

REFERENCES

[1] K. Kaygusuz, "Energy and environmental issues relating to greenhouse gas emissions for sustainable development in Turkey," *Renewable and Sustainable Energy Reviews*, vol. 13, no. 1, pp. 253–270, Jan. 2009, https://doi.org/10.1016/j.rser.2007.07.009.

[2] P. A. Owusu and S. Asumadu-Sarkodie, "A review of renewable energy sources, sustainability issues and climate change mitigation," *Cogent Engineering*, vol. 3, no. 1, Dec. 2016, Art. no. 1167990, https://doi.org/10.1080/23311916.2016.1167990.

[3] Y. Kassem, H. Camur, and E. G. Ghoshouni, "Assessment of a Hybrid (Wind-Solar) System at High-Altitude Agriculture Regions for achieving Sustainable Development Goals," *Engineering, Technology & Applied Science Research*, vol. 14, no. 1, pp. 12595–12607, Feb. 2024, https://doi.org/10.48084/etasr.6494.

[4] N. Vidadili, E. Suleymanov, C. Bulut, and C. Mahmudlu, "Transition to renewable energy and sustainable energy development in Azerbaijan," *Renewable and Sustainable Energy Reviews*, vol. 80, pp. 1153–1161, Dec. 2017, https://doi.org/10.1016/j.rser.2017.05.168.

[5] N. L. Panwar, S. C. Kaushik, and S. Kothari, "Role of renewable energy sources in environmental protection: A review," *Renewable and Sustainable Energy Reviews*, vol. 15, no. 3, pp. 1513–1524, Apr. 2011, https://doi.org/10.1016/j.rser.2010.11.037.

[6] Y. Kassem, H. Camur, and A. A. S. Mosbah, "Feasibility Analysis of the Wind Energy Potential in Libya using the RETScreen Expert," *Engineering, Technology & Applied Science Research*, vol. 13, no. 4, pp. 11277–11289, Aug. 2023, https://doi.org/10.48084/etasr.6007.

[7] H. S. A. Lagili, A. Kiraz, Y. Kassem, and H. Gökçekuş, "Wind and Solar Energy for Sustainable Energy Production for Family Farms in Coastal Agricultural Regions of Libya Using Measured and Multiple Satellite Datasets," *Energies*, vol. 16, no. 18, Jan. 2023, Art. no. 6725, https://doi.org/10.3390/en16186725.

[8] Y. Kassem, H. Gokcekus, and A. M. S. Essayah, "Wind Power Potential Assessment at Different Locations in Lebanon: Best–Fit Probability Distribution Model and Techno-Economic Feasibility," *Engineering, Technology & Applied Science Research*, vol. 13, no. 2, pp. 10578–10587, Apr. 2023, https://doi.org/10.48084/etasr.5686.

[9] M. A. Khan, H. Çamur, and Y. Kassem, "Modeling predictive assessment of wind energy potential as a power generation sources at some selected locations in Pakistan," *Modeling Earth Systems and Environment*, vol. 5, no. 2, pp. 555–569, Jun. 2019, https://doi.org/10.1007/s40808-018-0546-6.

[10] Y. Kassem, H. Gökçekuş, and W. Janbein, "Predictive model and assessment of the potential for wind and solar power in Rayak region, Lebanon," *Modeling Earth Systems and Environment*, vol. 7, no. 3, pp. 1475–1502, Sep. 2021, https://doi.org/10.1007/s40808-020-00866-y.

[11] Y. Kassem, H. Çamur, and M. A. H. A. Abdalla, "Predicting the Mechanical Power of a New-Style Savonius Wind Turbine Using Machine Learning Techniques and Multiple Linear Regression: Comparative Study," in *11th International Conference on Theory and Application of Soft Computing, Computing with Words and Perceptions and Artificial Intelligence - ICSCCW-2021*, Cham, Switzerland, 2022, pp. 316–323, https://doi.org/10.1007/978-3-030-92127-9_44.

[12] H. Fathabadi, "Novel grid-connected solar/wind powered electric vehicle charging station with vehicle-to-grid technology," *Energy*, vol. 132, pp. 1–11, Aug. 2017, https://doi.org/10.1016/j.energy.2017.04.161.

[13] M. N. F. Kamal *et al.*, "A Review of Aerodynamics Influence on Various Car Model Geometry through CFD Techniques," *Journal of Advanced Research in Fluid Mechanics and Thermal Sciences*, vol. 88, no. 1, pp. 109–125, Oct. 2021, https://doi.org/10.37934/arfmts.88.1.109125.

[14] M. N. Sudin, M. A. Abdullah, F. R. Ramli, M. T. Musthafa, and S. A. Shamsudin, "Review of research on vehicles aerodynamic drag reduction methods.," *International Journal of Mechanical and Mechatronics Engineering*, vol. 14, no. 2, pp. 35–47, Apr. 2014.

[15] J. Piechna, "A Review of Active Aerodynamic Systems for Road Vehicles," *Energies*, vol. 14, no. 23, Jan. 2021, Art. no. 7887, https://doi.org/10.3390/en14237887.

[16] I. Gypa, M. Jansson, R. Gustafsson, S. Werner, and R. Bensow, "Controllable-pitch propeller design process for a wind-powered car-carrier optimising for total energy consumption," *Ocean Engineering*, vol. 269, Feb. 2023, Art. no. 113426, https://doi.org/10.1016/j.oceaneng.2022.113426.

[17] H. Çamur and Y. Kassem, "Creating the Wind Energy for Operating the 3-C-Section Blades Wind Car," *Advanced Materials Research*, vol. 622–623, pp. 1188–1193, 2013, https://doi.org/10.4028/www.scientific.net/AMR.622-623.1188.

[18] H. Çamur and Y. Kassem, "Operating a Three Blade-Wind Car with Wind Energy," *Advanced Materials Research*, vol. 622–623, pp. 1199–1203, 2013, https://doi.org/10.4028/www.scientific.net/AMR.622-623.1199.

[19] G. Quartey and S. Adzimah, "Generation of Electrical Power by a Wind Turbine for Charging Moving Electric Cars," *Journal of Energy Technologies and Policy*, vol. 4, no. 3, pp. 19–29, 2014.

[20] Y. Kassem and H. Çamur, "Wind Turbine Powered Car Uses 3 Single Big C-Section Blades," in *International Conference on Aeronautical And Manufacturing Engineering*, Dubai, UAE, Mar. 2015, https://doi.org/10.15242/IAE.IAE0315209.

[21] Y. Kassem, H. Çamur, and A. Alghazali, "Prediction of the Mechanical Power in Wind Turbine Powered Car UsingVelocity Analysis," *American Journal of Science, Engineering and Technology*, vol. 3, no. 1, pp. 10–20, Mar. 2018, https://doi.org/10.11648/j.ajset.20180301.12.

[22] Y. Kassem, "Computational study on vertical axis wind turbine car: static study," *Modeling Earth Systems and Environment*, vol. 4, no. 3, pp. 1041–1057, Sep. 2018, https://doi.org/10.1007/s40808-018-0461-x.

[23] F. Arbiyani and F. P. Lasut, "Design of Savonius Vertical Axis Wind Turbine for Vehicle," *Journal of Mechanical Engineering Science and Technology*, vol. 4, no. 2, pp. 125–134, Nov. 2020, https://doi.org/10.17977/um016v4i22020p125.

[24] M. A. H. Mohamad and Y. Kassem, "Influence Of Size And Number Of Naca 0012 Blades On The Mechanical Power Of Wind Turbine-Powered Car," *Open Access Repository*, vol. 10, no. 6, pp. 68–86, Jun. 2023, https://doi.org/10.17605/OSF.IO/UXF8G.

[25] J. Chapa, "Greenbird wind powered vehicle breaks world record," *The Guardian*, Apr. 01, 2009.

[26] University of Stuttgart, "Wind Powered Vehicle, Ventomobile, Ready To Race In The Netherlands," *Science Daily*, Aug. 06, 2008.

[27] J. Stewart, "Blackbird Wind-powered car sails against the storm," *BBC Future*, Feb. 24, 2022.

[28] A. George, "Windmill Manufacturer Builds an EV Coupe That Looks Suspiciously Familiar," *Wired*, Sep. 25, 2012.

[29] A. H. Rajpar, I. Ali, A. E. Eladwi, and M. B. A. Bashir, "Recent Development in the Design of Wind Deflectors for Vertical Axis Wind Turbine: A Review," *Energies*, vol. 14, no. 16, Jan. 2021, Art. no. 5140, https://doi.org/10.3390/en14165140.

[30] R. Howell, N. Qin, J. Edwards, and N. Durrani, "Wind tunnel and numerical study of a small vertical axis wind turbine," *Renewable Energy*, vol. 35, no. 2, pp. 412–422, Feb. 2010, https://doi.org/10.1016/j.renene.2009.07.025.

[31] X. Sun, Y. Chen, Y. Cao, G. Wu, Z. Zheng, and D. Huang, "Research on the aerodynamic characteristics of a lift drag hybrid vertical axis wind turbine," *Advances in Mechanical Engineering*, vol. 8, no. 1, pp. 1–11, Jan. 2016, https://doi.org/10.1177/1687814016629349.

[32] N. H. Mahmoud, A. A. El-Haroun, E. Wahba, and M. H. Nasef, "An experimental study on improvement of Savonius rotor performance," *Alexandria Engineering Journal*, vol. 51, no. 1, pp. 19–25, Mar. 2012, https://doi.org/10.1016/j.aej.2012.07.003.

[33] S. McTavish, D. Feszty, and T. Sankar, "Steady and rotating computational fluid dynamics simulations of a novel vertical axis wind turbine for small-scale power generation," *Renewable Energy*, vol. 41, pp. 171–179, May 2012, https://doi.org/10.1016/j.renene.2011.10.018.

[34] A. Rezaeiha, H. Montazeri, and B. Blocken, "Towards accurate CFD simulations of vertical axis wind turbines at different tip speed ratios and solidities: Guidelines for azimuthal increment, domain size and convergence," *Energy Conversion and Management*, vol. 156, pp. 301–316, Jan. 2018, https://doi.org/10.1016/j.enconman.2017.11.026.

[35] D. S. Nath, P. C. Pujari, A. Jain, and V. Rastogi, "Drag reduction by application of aerodynamic devices in a race car," *Advances in Aerodynamics*, vol. 3, no. 1, Jan. 2021, Art. no. 4, https://doi.org/10.1186/s42774-020-00054-7.

[36] V. Kshirsagar and J. V. Chopade, "Aerodynamics of high performance vehicles," *International Research Journal of Engineering and Technology (IRJET)*, vol. 5, no. 3, pp. 2182–2186, Mar. 2018.

[37] G. Larose, L. Belluz, I. Whittal, M. Belzile, R. Klomp, and A. Schmitt, "Evaluation of the Aerodynamics of Drag Reduction Technologies for Light-duty Vehicles: a Comprehensive Wind Tunnel Study," *SAE International Journal of Passenger Cars - Mechanical Systems*, vol. 9, no. 2, pp. 772–784, Apr. 2016, https://doi.org/10.4271/2016-01-1613.

[38] B. G. D. C. Budgeta, "Analysis of car body aerodynamics with variation of speed using CFD software," *Satukata: Jurnal Sains, Teknik, dan Studi Kemasyarakatan*, vol. 1, no. 1, pp. 27–32, Dec. 2022.

[39] M. Yusaiyin and N. Tanaka, "Effects of windbreak width in wind direction on wind velocity reduction," *Journal of Forestry Research*, vol. 20, no. 3, pp. 199–204, Sep. 2009, https://doi.org/10.1007/s11676-009-0039-6.

[40] K. Grogg, "Harvesting the Wind: The Physics of Wind Turbines," *Carleton Digital Commons*, 2005

[41] H. Aboujaoude, F. Beaumont, S. Murer, G. Polidori, and F. Bogard, "Aerodynamic performance enhancement of a Savonius wind turbine using an axisymmetric deflector," *Journal of Wind Engineering and Industrial Aerodynamics*, vol. 220, Jan. 2022, Art. no. 104882, https://doi.org/10.1016/j.jweia.2021.104882.

[42] T. G. Shanegowda, C. M. Shashikumar, V. Gumtapure, and V. Madav, "Comprehensive analysis of blade geometry effects on Savonius hydrokinetic turbine efficiency: Pathways to clean energy," *Energy Conversion and Management: X*, vol. 24, Oct. 2024, Art. no. 100762, https://doi.org/10.1016/j.ecmx.2024.100762.

[43] A. G. Chitura, P. Mukumba, and N. Lethole, "Enhancing the Performance of Savonius Wind Turbines: A Review of Advances Using Multiple Parameters," *Energies*, vol. 17, no. 15, Jan. 2024, Art. no. 3708, https://doi.org/10.3390/en17153708.

[44] M. A. Kamoji, S. B. Kedare, and S. V. Prabhu, "Performance tests on helical Savonius rotors," *Renewable Energy*, vol. 34, no. 3, pp. 521–529, Mar. 2009, https://doi.org/10.1016/j.renene.2008.06.002.

[45] U. K. Saha, S. Thotla, and D. Maity, "Optimum design configuration of Savonius rotor through wind tunnel experiments," *Journal of Wind Engineering and Industrial Aerodynamics*, vol. 96, no. 8, pp. 1359–1375, Aug. 2008, https://doi.org/10.1016/j.jweia.2008.03.005.

[46] A. Barnes, D. Marshall-Cross, and B. R. Hughes, "Towards a standard approach for future Vertical Axis Wind Turbine aerodynamics research and development," *Renewable and Sustainable Energy Reviews*, vol. 148, Sep. 2021, Art. no. 111221, https://doi.org/10.1016/j.rser.2021.111221.

[47] R. Kumar, K. Raahemifar, and A. S. Fung, "A critical review of vertical axis wind turbines for urban applications," *Renewable and Sustainable Energy Reviews*, vol. 89, pp. 281–291, Jun. 2018, https://doi.org/10.1016/j.rser.2018.03.033.

[48] H. Guo, X. Zhou, and Z. Liu, "Advanced Lightweight Structural Materials for Automobiles: Properties, Manipulation, and Perspective," *Science of Advanced Materials*, vol. 16, no. 5, pp. 563–580, May 2024, https://doi.org/10.1166/sam.2024.4686.

[49] Q. Hassan, S. Algburi, A. Z. Sameen, H. M. Salman, and M. Jaszczur, "A review of hybrid renewable energy systems: Solar and wind-powered solutions: Challenges, opportunities, and policy implications," *Results in Engineering*, vol. 20, Dec. 2023, Art. no. 101621, https://doi.org/10.1016/j.rineng.2023.101621.